Seatific, Vol. 3, Issue. 2, pp. 51–70, December 2023

Seatific Journal
https://seatific.yildiz.edu.tr
DOI: https://doi.org/10.14744/seatific.2023.0007

Research Article

A domestic waste heat recovery system: Mathematical model of a green kitchen module

Stefano Maria SPAGOCCI*

SMS Consulting, Cinisello Balsamo (MI), Italy

ARTICLE INFO

Article history
Received: March 20, 2023
Revised: July 27, 2023
Accepted: September 11, 2023

Key words:
Appliances; energy saving; phase change materials; sensible heat materials

ABSTRACT

A lumped parameter model of a domestic heat storage/recovery system is described. This is a typical green kitchen application, where the heat dissipated by kitchen appliances is stored in suitable materials by temperature rise and/or phase transitions. To this aim, sensible heat materials and phase change materials are considered. Based on the model, a number of design solutions are proposed, making use of fixed beds or shell-and-tube heat exchangers, where heat is stored in spheres or cylinders made up of (or encapsulating) suitable materials. The best solution (a PCM-based shell-and-tube exchanger) corresponds to ~50×50×25 cm, ~30 kg modules.

Cite this article as: Spagocci SM. A domestic waste heat recovery system: Mathematical model of a green kitchen module. Seatific 2023;3:2:51–70.

1. INTRODUCTION

The present environmental concerns, and the fact that the conventional energy sources are bound to be exhausted, make the search of alternative energy sources more urgent than ever. Energy saving is a form of alternative energy; in this context, waste heat recovery becomes particularly important. To appreciate the importance of this form of energy saving, one can consider the fact that in the UK alone 40 TWh per year could come from waste heat recovery in the industrial sector [MOXOFF, 2012a]. In this paper, the results obtained in a design study of heat storage/recovery systems (aimed at green kitchen applications) are described, together with the model employed to achieve them. In the green kitchen approach [MOXOFF, 2013a - Mukherjee, 2011], the thermal energy dissipated by various kitchen appliances is recovered by various means, typically for the production of hot water for domestic use.

There are various forms of waste heat recovery [Hussam et al., 2018]: regenerative and recuperative burners [Institute for Industrial Productivity, 2017 - BDF Industries, 2017] capture the waste heat from the combustion of hot flue gases, economizers [Thermtech, 2014] recover waste heat to be used for heating liquids, waste heat boilers [Ganapathy, 2015] are suitable to recover heat from exhaust gases and mainly used to produce steam for power generation, air preheaters [Yodrak et al., 2010] are employed for exhaust heat recovery. Heat exchangers [IPIECA, 2022] and heat pipes [JHCSS, 2017] are employed in such devices. The recovered heat can be employed to preheat the gases entering burners and/or furnaces, to produce electricity by steam or thermoelectric generators. In green kitchen applications the recovered waste heat comes from domestic appliances.

To have an idea of the potentialities of such technologies, one can consider the fact that savings of the order of 5-10% can be achieved by preheating gases in burners [Spirax Sarco, 2011], producing steam via a Rankine cycle can reach an efficiency of 22% [Stefanou, 2017], thermoelectric generators have a 2-5% efficiency but through the use of nanotechnologies efficiencies greater than 15% can be achieved [Caillat et al., 1999].

***Corresponding author.**
*E-mail address: scimodsim@gmail.com, stefanspag@gmail.com

In regenerative burners, the heat coming from the hot flue gases is first stored in a heat exchange medium such as aluminum oxide, then recovered by heating the cold gas through contact with the medium: this is an example of the utility of sensible heat materials in waste heat recovery. Sensible heat materials [Sarbu et al., 2018] store heat by increasing their temperature; in phase change material [Sarbu et al., 2018 - Ahmed et al., 2018], energy is mainly stored in the form of latent heat, although there can also be a temperature increase. Among sensible heat materials one can cite water, rock, sand and steel. Phase change materials can be classified as organic (paraffins and non-paraffins), inorganic (salt hydrates, low melting point metals), eutectic mixtures. At present, the cheapest and more performant phase change materials are paraffins [Sarbu et al., 2018].

In this paper, the lumped-parameter model employed is first described. To the best of the author's knowledge, this model substantially innovates the existing literature. On the base of the developed model, a number of solutions are proposed. The focus is on a thermal bus, with a refrigerator, an induction cook-top and a domestic oven connected in series. Whirlpool Europe presented a patent application [Mukherjee, 2011] concerning a green kitchen heat storage/recovery system, based on a water tank as the storage medium. The use of cylindrical modules, with cylindrical or spherical storage modules, was only proposed as an ancillary system, improving the water tank performance. The system described here, whose feasibility study was commissioned by Whirlpool Europe, substantially improves the solution proposed in the patent. In the main body of the paper, the formulae needed for practical use are only given; a full treatment is in Annexes A1-A7.

2. PROBLEM SETTING

In Table 1, some typical sensible heat materials (SHMs) and phase change materials (PCMs) are illustrated. The table shows that the energy storage density for PCMs is up to ~10 times larger than for SHMs. For appliance temperatures <50°C, the module charging process has to stop before the onset of fusion. In this case, PCMs only count for their specific heat. In this temperature range, SHMs may be more suitable than PCMs.

The first proposed approach is based on sensible heat materials [Dincer et al., 1997 - Sharma et al., 2005]. In this approach, the dissipated heat, carried by a fluid, heats the material. In the heat recovery phase, a cold fluid is put in touch with the material and heats up. If ρ_m is the material density, C its specific heat, ΔT the difference between the fluid and solid temperatures, then the material energy density is:

$$\rho_e=\rho_m \cdot C \cdot \Delta T \quad (1)$$

In Table 2, the thermophysical properties of typical SHMs are shown.

Phase change materials [Sharma et al., 2009] work similarly, except that most of the thermal energy is accumulated in the form of latent heat of fusion. During the phase transition, the material does not change its temperature. If ρ_m is the material density, ΔH the transition (fusion) enthalpy, the material energy density is:

$$\rho_e=\rho_m \cdot \Delta H \quad (2)$$

In Table 3, the thermophysical properties of common PCMs are shown.

In heat storage/recovery systems, the storage material is part of a heat exchanger so that, in the module charging phase, a hot thermo-vector fluid (heated by the thermal energy to recover) is able to transfer heat to the material. In the module discharging phase, a cold thermo-vector fluid gets heated, removing heat from the material.

In [MOXOFF, 2013a - Mukherjee, 2011], a possible design solution, based on a fixed bed (Fig. 1), was proposed. A fixed bed [Holdich, 2002] is a metal cylinder, filled with spheres of a suitable material and crossed by a thermo-vector fluid that exchanges heat with them. In the fixed bed regime, the viscous drag force does not prevail over gravity and the spheres are stuck in their position. Beyond the minimal fluidization velocity, the viscous drag force overcomes gravity and the spheres acquire a turbulent motion. One is then in the fluidized bed regime; the latter is unstable for spheres of diameter ≥1 cm [Holdich, 2002]. The diameter that had to be chosen falls in this range [MOXOFF, 2013b]; consequently, a fluidized bed solution was not considered.

In [MOXOFF, 2013a - Mukherjee, 2011] a possible design solution, based on a shell-and-tube heat exchanger [Mukherjee, 1998] (Fig. 2), was also proposed. Here it is only pointed out that the shell-and-tube heat exchanger has to be equipped with baffles, whose aim is described later. In [MOXOFF, 2013a], appliances are classified, according to their time behaviour, as discrete or continuous. As an example, one may consider a domestic oven and a refrigerator. Heat is recovered from a domestic oven when the appliance is turned off and its temperature is ~180-250°C [Zavattoni, 2012]. One then has a discrete process. A refrigerator, instead, dissipates energy continuously. A typical refrigerator is reported to dissipate 84 W at 40°C [Zavattoni, 2012].

Appliances can either dissipate at a nearly constant temperature (as in the case of a refrigerator or cook-top induction plane) or a variable temperature (as in the case of a domestic oven). The following module classification is then proposed:

- Constant Inlet Temperature Modules with SHMs (CITSHM),
- Constant Inlet Temperature Modules with PCMs (CITPCM),
- Variable Inlet Temperature Modules with SHMs (VITSHM),
- Variable Inlet Temperature Modules with PCMs (VITPCM).

Table 1. Heat storage characteristics of typical materials [Dincer, 1997 - Sharma et al., 2009]. ΔT = 15°C is assumed for sensible heat materials

Property	Rock	Water	Organic PCM	Inorganic PCM
Density (kg/m^3)	2240	1000	800	1600
Specific heat (kJ/kg.°K)	1.00	4.18	2.00	2.00
Latent heat (kJ/kg)	-	-	190	230
Mass per 10^6 J stored (kg)	67	16	5.30	4.35
Volume per 10^6 J stored (m^3)	30	16	6.60	2.70
Relative mass	15	4	1.25	1.00
Relative volume	11	6	2.50	1.00

PCM: Phase change materials

Table 2. Heat storage characteristics of typical sensible heat materials [Dincer, 1997 - Mardiana-Idayua et al., 2012]

Material	Water	Aluminum	Rock	Steatite	Steel
Density (kg/m^3)	1000	2700	2560	2680	7800
Specific heat (kJ/kg.°K)	4.18	0.90	0.96	1.07	0.57
Thermal conductivity (W/m.°K)	0.60	204	0.48	2.50	50

Table 3. Thermophysical properties of various phase change materials [Sharma et al., 2005 - Sharma et al., 2009]. The literature data are inconsistent and fragmentary. Where a parameter is available for only one phase, the value for the remaining phase was taken to coincide with the available value. Where a piece of data is missing for both phases, when possible, it was approximated with the average value for materials of the same category, when not possible, it was approximated with the typical values of Table 1. In the case of inconsistent data from different sources, the most pessimistic value was chosen. Materials with a transition temperature in the 20-100°C range were only considered. (l) = liquid state, (s) = solid state

Material	Fusion temperature (°C)	Fusion heat (kJ/kg)	Thermal conductivity (l) (W/m.°K)	Thermal conductivity (s) (W/m.°K)	Density (l) (kg/m^3)	Density (s) (kg/m^3)	Specific heat (l) (kJ/kg.°K)	Specific heat (s) (kJ/kg.°K)
Paraffin C16-C28	42	189.0	0.210	0.210	765	765	2.100	2.100
Paraffin C20-C33	48	189.0	0.210	0.210	769	769	2.100	2.100
N-Hexacosane	56	257.0	0.210	0.210	770	770	2.100	2.100
Paraffin C22-C45	58	189.0	0.210	0.210	795	795	2.100	2.100
Paraffin C23-C45	62	189.0	0.210	0.210	790	790	2.100	2.100
Paraffin wax	64	173.6	0.167	0.339	790	790	2.100	2.100
Paraffin C21-C50	66	189.0	0.210	0.210	830	830	2.100	2.100
Naphtalene	80	147.7	0.132	0.34	976	976	2.000	2.000
$Ba(OH)_2 . 8H_2O$	48	265.0	0.653	0.653	1937	1937	2.000	2.000
$Mg(NO_3)_2 . 6H_2O$	89	149.5	0.490	0.490	1550	1550	2.000	2.000
$Mg(NO_3)_2 . 6H_2O + NH_4NO_3$	52	125.5	0.494	0.494	1515	1515	2.000	2.000
Naphtalene + Benzoic acid	67	123.4	0.130	0.257	800	800	2.000	2.000
Lauric acid	42	178.0	0.147	0.147	870	870	1.600	1.600
Stearic acid	60	186.5	0.172	0.172	848	848	2.350	2.350
Palmitic acid	61	185.4	0.132	0.132	848	989	1.975	1.975
Neopentylglycol	48	139.0	0.360	0.360	1190	1190	2.760	2.760
Trimethylol ethane	82	174.0	0.510	0.510	1220	1220	2.750	2.00

3. MATHEMATICAL MODEL

3.1. System dimensioning

In order to be able to calculate the dimensions of the proposed heat storage/recovery systems, let us first introduce the energy size E_0, scaled by a factor f_d (whose aim is clarified in the following). The volume of material needed to achieve an energy size E_0 can then be calculated based on ρ_e, the storage density, Eq. (1) or (2). In particular, one has:

$$V_m = \frac{f_d \cdot E_0}{\rho_e} \quad (3)$$

Let us also introduce the porosity 1-ε_3, for a fixed bed and a shell-and-tube exchanger. In the former case, one has to use the result reported in the literature for the maximum

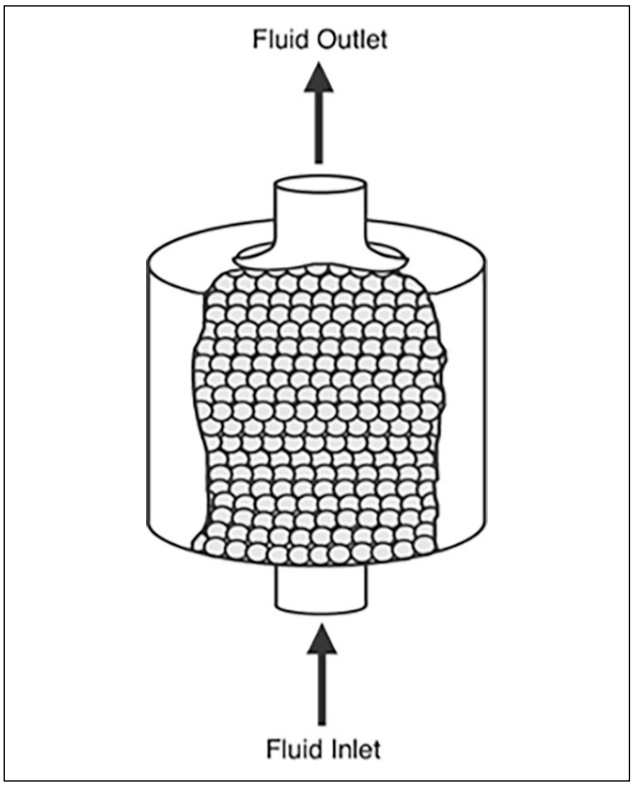

Figure 1. A heat storage/recovery module, based on a fixed bed. The spheres are filled with a phase change material (such as glycol) or made up of a sensible heat material (such as aluminium).

sphere packing density (face-centered cubic lattice [Hales et al., 2006]).

In particular, one has

$$\varepsilon_3 = \frac{\pi}{3\cdot\sqrt{2}} \approx 74\% \quad (4)$$

Provided this is economically feasible, spheres in the fixed bed could be packed according to Eq. (4), at least approximately. The random sphere packing density is instead ~64% [Song et al., 2008] so, cautiously, this figure was rather employed. For cylinder packing, ε_3 can be calculated analytically, under the hypothesis that each circle of radius ru is located at the center or edges of a square of size $4\cdot r_u$ and each cell contains two circles. One has to consider that, in shell-and-tube exchangers, an empirical rules states that for greater efficiency the tube pitch (minimum distance between the tubes) must be 1.25 times their diameter [Mukherjee, 1998]:

$$\varepsilon_3 = \frac{4\pi}{25} \approx 50\% \quad (5)$$

A porosity $1\text{-}\varepsilon_2$, characterizing the average velocity of the thermo-vector fluid in the fixed bed, can finally be defined and it turns out that:

$$\varepsilon_2 = \varepsilon_3 \quad (6)$$

as shown by the continuity equation [Sharma et al., 2005]. The module volume is then:

$$V_c = \frac{V_m}{\varepsilon_3} \quad (7)$$

Let us also define the shape factors a_c and a_u, for a cylindrical module of height h_c and the module or its storage units, respectively:

$$a_c = \frac{h_c}{r_c} \quad (8)$$

and:

$$a_u = \frac{h_c}{r_u} \quad (9)$$

One can then calculate N_u, the number of heat storage units, for spheres and cylinders. The calculation can be carried out by noticing that the total volume occupied by the storage units is given by $V_c\cdot\varepsilon_3$ and dividing this volume by the volume of a single storage unit. For spheres, one has:

$$N_u = \frac{\pi}{\sqrt{32}}\cdot\frac{a_u^3}{a_c^2} \quad (10)$$

for perfect packing (in the case of random packing, the coefficient is ~0.48). For cylinders:

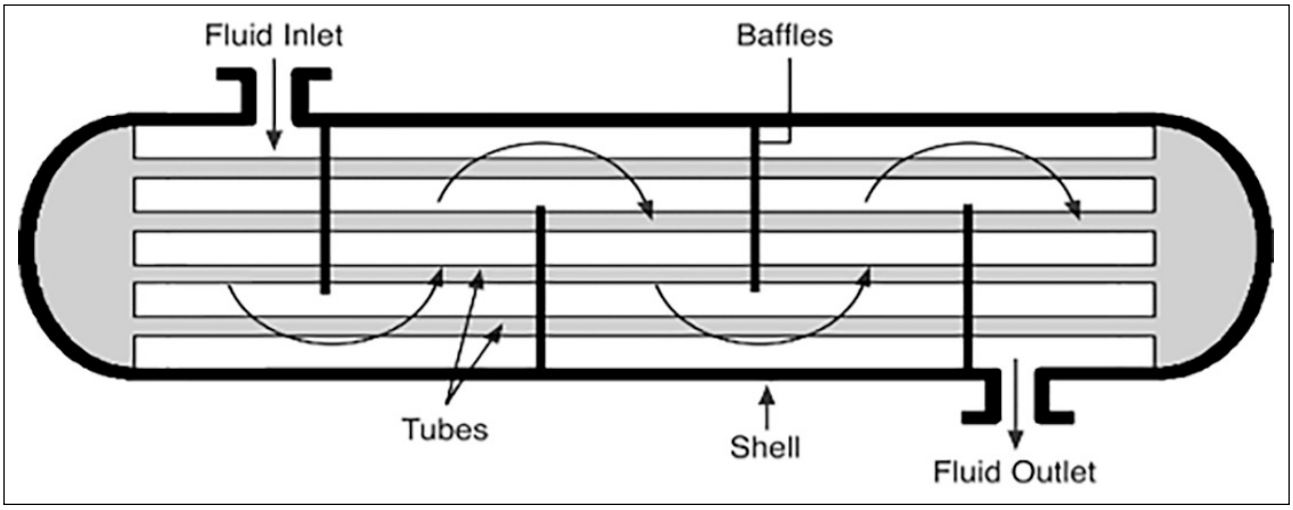

Figure 2. A heat storage/recovery module, based on a shell-and-tube heat exchanger. The spheres are filled with a phase change material (such as glycol) or made up of a sensible heat material (such as aluminium).

Table 4. The PCM-based fixed bed heat storage/recovery system. The system is made up of four thermally insulated modules. There are two parallel refrigerator modules, alternatively working in the charging and discharging mode. System diameter = 50 cm. Spherical heat storage unit diameter = 1 cm. Charging time = 18 min. Effective charge efficiency = 145%. Energy efficiency = 80%

	Compound	Height (cm)	Mass (kg)	Energy storage (MJ)	Air flow (l/s)	Number of units
Induction plane (18 min, 100 W @ 60°C)	Glycol	4.0	5.9	0.1	2.4	12633
Oven (18 min, 365 W @ 80°C)	Glycol	4.7	7.1	1.1	5.9	15220
Refrigerator (18 min, 84 W @ 40°C)	Glycol	2×3.9	2×5.9	2×0.1	2 x 4.0	2×12561
Total (549 W)		16.5	24.8	1.4	16.3	52975

Table 5. The PCM-based shell-and-tube heat storage/recovery system. The system is made up of four thermally insulated modules. There are two parallel refrigerator modules, alternatively working in the charging and discharging mode. System diameter = 50 cm. Cylindrical heat storage unit diameter = 0.5 cm. Charging time = 18 min. Effective charge efficiency = 122%. Energy efficiency = 76%

	Compound	Height (cm)	Mass (kg)	Energy storage (MJ)	Air flow (l/s)	Number of units
Induction plane (18 min, 100 W @ 60°C)	Glycol	5.7	6.7	0.1	2.4	5027
Oven (18 min, 365 W @ 80°C)	Glycol	5.6	6.6	1.1	5.9	5027
Refrigerator (18 min, 84 W @ 40°C)	Glycol	2×6.2	2×7.3	2×0.1	2×4.0	2×5027
Total (549 W)		23.9	27.9	1.4	16.3	20108

$$N_u = \frac{4\pi}{25} \cdot \frac{a_u^3}{a_c^2} \tag{11}$$

On the other hand, S_u, the total heat exchange area of the units, is easily determined by multiplying the exchange area of a storage unit by the number of units. For spheres:

$$S_u = \frac{\pi^2}{\sqrt{2}} \cdot a_u \cdot r_c^2 \tag{12}$$

and for cylinders:

$$S_u = \frac{8\pi^2}{25} \cdot \frac{a_u}{a_c} \cdot h_c \cdot r_c \tag{13}$$

For the best solutions, it was determined that $N_u \approx 20000$ (cylindrical storage modules) and $N_u \approx 50000$ (spherical storage modules). See Tables 4-7.

3.2. Thermal energy exchange

Let us then present the model devised for calculating the heat storage/recovery system features, which generalizes the results in [Bejan, 1978]. To this aim, let us first introduce the quantity:

$$\tau = \frac{M \cdot C}{\dot{m} \cdot C_p} \tag{14}$$

with dimensions of time, where M is the heat storage material mass, C its effective specific heat, $\dot{m}$ the mass flow rate of the thermo-vector fluid, C_p its specific heat. Let us then introduce θ (non-dimensional time) and y, given by:

$$\theta = \frac{t}{\tau} \tag{15}$$

$$y = 1 - exp(-NTU) \tag{16}$$

where NTU (the Number of Transfer Units) is a non-dimensional parameter, given by:

$$NTU = \frac{U \cdot S_u}{\dot{m} \cdot C_p} \tag{17}$$

In Eq. (17), U is the heat exchange coefficient. For our geometry and fluid, it turns out that NTU>>1. As a consequence of Eq. (16), one has y≈1. Also, in Annex A3 it is shown that NTU>>1 maximizes the system effectiveness. Therefore, this condition was imposed to our solutions. As for the temperature profile, one has:

$$T = T_\infty + (T_0 - T_\infty) \cdot exp(-\theta) + \Delta T(t) \tag{18}$$

with:

$$\Delta T(t) = exp(-\theta) \cdot \int_0^\theta ds \cdot exp(s) \cdot \Delta T_\infty(s) \tag{19}$$

$$\Delta T_\infty(t) = T_{in}(t) - T_\infty \tag{20}$$

In the previous equations:

- T is the material (fluid outlet) temperature,
- T_0 is the room temperature,
- $T_{in}(t)$ is the temperature of the thermo-vector fluid at the inlet,
- T_∞ is the asymptotic value of $T_{in}(t)$.

Let us observe that the material and, as explained, fluid outlet temperatures, for y≈1 are almost equal [Wall, 1977].

Table 6. The SHM-based fixed bed heat storage/recovery system. The system is made up of four thermally insulated modules. There are two parallel refrigerator modules, alternatively working in the charging and discharging mode. System diameter = 50 cm. Spherical heat storage unit diameter = 1 cm. Charging time = 18 min. Effective charge efficiency = 87%. Energy efficiency = 87%

	Compound	Height (cm)	Mass (kg)	Energy storage (MJ)	Air flow (l/s)	Number of units
Induction plane (18 min, 100 W @ 60°C)	Aluminium	5.5	18.2	0.1	2.4	17151
Oven (18 min, 365 W @ 80°C)	Aluminium	14.9	50.6	1.1	5.9	47763
Refrigerator (18 min, 84 W @ 40°C)	Aluminium	2×5.3	2×18.1	2×0.1	2×4.0	2×17053
Total (549 W)		31.0	105.0	1.4	16.3	99020

Table 7. The SHM-based shell-and-tube heat storage/recovery system. The system is made up of four thermally insulated modules. There are two parallel refrigerator modules, alternatively working in the charging and discharging mode. System diameter = 50 cm. Heat storage cylindrical unit diameter = 0.5 cm. Charging time = 18 min. Effective charge efficiency = 83%. Energy efficiency = 83%

	Compound	Height (cm)	Mass (kg)	Energy storage (MJ)	Air flow (l/s)	Number of units
Induction plane (18 min, 100 W @ 60 °C)	Aluminium	7.7	20.6	0.1	2.4	5027
Oven (18 min, 365 W @ 80 °C)	Aluminium	17.7	47.1	1.1	5.9	5027
Refrigerator (18 min, 84 W @ 40 °C)	Aluminium	2×8.5	2×22.6	2×0.1	2×4.0	2×5027
Total (549 W)		42.4	112.9	1.4	16.3	20108

T_∞ coincides with the appliance dissipation temperature, for constant temperature appliances. For variable temperature, it coincides with the asymptotic temperature of the fluid and the module. See Annexes for details.

As for the appliance temperatures, the relevant cases are both constant and exponentially decreasing dissipation temperatures [MOXOFF, 2013b]. In particular, the exponential law applies to convection oven cooling, where, as demonstrated in Annex A2, things work as if the oven dissipated at an effective and constant temperature. In all practically relevant cases, Eqs. (18) to (20) then reduce to [Bejan, 1978]:

$$T=T_\infty+(T_0-T_\infty)\cdot exp(-\theta) \quad (21)$$

where T describes both the fluid outlet and material temperature and T_∞, in the case of a domestic oven, must be interpreted as an effective temperature. Eq. (21) reveals that, for short charging times, both the outlet fluid and the material are at room temperature. Their temperature increases exponentially, until both reach the inlet fluid temperature. For long charging times, the heat transfer rate between the material and the fluid becomes negligible, since they approximately reach the same temperature.

By introducing the concept of exergy [Bjurström et al., 1985], defined as the maximum work that a system can do while reaching equilibrium with its environment, and exergetic efficiency, it is then possible to maximize the system exergetic efficiency (Annex A5) as a function of charge time. The thermodynamic optimization translates into an expression for T_{opt}, the optimal module charging temperature. In fact, such a temperature is approximately given by the geometric mean between the room and fluid inlet temperatures. In [Bjurström et al., 1985] it is stated that this geometric mean approximates the optimal charging temperature when the module temperature increase is negligible. As detailed in Annex A6, such an expression (at 5%) rather describes T_{opt} in the 20-100°C range, so that:

$$T_{opt}\approx\sqrt{T_0\cdot T_\infty} \quad (22)$$

Let us point out that, in the interval 20-100°C, the arithmetic and geometric means differ by ~1%. More accurately, in the 20-100°C range one has (Annex A6):

$$T_{opt}=0.64\cdot T_\infty+0.36\cdot T_0 \quad (23)$$

By inverting Eq. (23), one finds an expression for the system charging time:

$$T_{opt}=\frac{\tau}{f_d}\cdot log(\frac{T_\infty-T_0}{T_\infty-T_{opt}}) \quad (24)$$

where τ is given by Eq. (14), T_{opt} by Eq. (23) and the factor f_d was inserted. Let us notice that, by substituting Eq. (23) in Eq. (24), it is seen that $t_{opt}\approx\tau$ (provided f_d=1). For the optimal

configurations, then, θ≈1. As explained below, by over-dimensioning the module by the factor f_d, it is possible to achieve an apparent charging efficiency of more than 100%.

Since an infinitesimal fluid volume, entering the heat exchanger at T_∞ and transferring its thermal energy to the storage material, exits the system and suddenly reaches T_0 [Wall, 1977], it is possible to establish a relationship between the mass flow rate and the power transported by the fluid:

$$W=\dot{m}\cdot C_p\cdot(T_\infty-T_0) \tag{25}$$

This expression then allows to determine the volume throughput Φ, given W:

$$\Phi=\frac{W}{p_m\cdot C_p\cdot(T_\infty-T_0)} \tag{26}$$

Given Eq. (25) and:

$$E=M\cdot C\cdot(T_\infty-T_0) \tag{27}$$

(E=fd·E0) the system time constant, Eq. (16), can be re-written as:

$$\tau=\frac{E}{W} \tag{28}$$

From Eq. (24), then:

$$T_{opt}=\frac{E_0}{W}\cdot log(\frac{T_\infty-T_0}{T_\infty-T_{opt}}) \tag{29}$$

One also needs to calculate U, the thermal exchange coefficient. For fixed beds, the correlation in [Chauk et al., 1998] was employed:

$$N_u=\frac{U.(2.r_u)}{k_f}=1.80\cdot(Pr)^{1/3}\cdot(\mathrm{Re})^{1/2} \tag{30}$$

For the shell-and-tube exchangers [Fernandez et al., 2010]:

$$N_u=\frac{U.(2.r_u)}{k_f}=1.04\cdot(Pr)^{0.36}\cdot(\mathrm{Re})^{0.40} \tag{31}$$

In the previous equations, N_u is the Nusselt number, k_f the thermal conductivity of the fluid, Pr the Prandtl number [Dincer et al., 1997 - Fernandez et al., 2010]:

$$Pr=\frac{\mu_f\cdot C_p}{k_m} \tag{32}$$

where μ_f is the viscosity of the thermo-vector fluid, k_m is the thermal conductivity of the material and Re is the Reynolds number [Chauk et al., 1998 - Shah et al., 1998]:

$$\frac{\rho_m\cdot(1-\epsilon_3)\cdot(2\cdot r_u)\cdot v_f}{\mu_f} \tag{33}$$

where v_f is the thermo-vector fluid mean velocity. For Re>3000 one enters the turbulent regime [Shah et al., 1998]. In our case, Re<1200 [MOXOFF, 2012b]. The mean thermo-vector fluid velocity is:

$$v_f=\frac{\Phi}{f_p(1-\epsilon_2)\cdot\pi\cdot r_c^2} \tag{34}$$

where f_p is the ratio between baffle pitch and cylinder diameter (0.051, corresponding to a baffle pitch of 1 in and a cylinder diameter of 50 cm [MOXOFF, 2013b]).

In order to quantify the efficiency of green kitchen modules, let us introduce:

- the charge efficiency η_c, defined as the ratio between the stored energy and the maximum energy that could be stored in the system (its energy size E_0),
- the energetic efficiency η_e, defined as the ratio between the energy stored and the energy transported by the thermo-vector fluid.

As shown later, both indicators have to be considered, in order to quantify the system behaviour. In particular, one has:

$$\eta_c=\frac{M\cdot C\cdot(T-T_0)}{M\cdot C\cdot(T_\infty-T_0)}=1-\exp(-\theta) \tag{35}$$

$$\eta_e=\frac{M\cdot C\cdot(T-T_0)}{\mathrm{W}\cdot t}=\frac{\eta_c}{\theta}=\frac{1-\exp(-\theta)}{\theta} \tag{36}$$

Let us point out that ηc monotonically increases from 0 to 1, as t→∞. For finite charging times, then, η_c<1. In fact, ηc could be made ≈1, provided t→∞. In this case, however, η_e→0. In fact, η_e monotonically decreases from 1 to 0, as t→∞.

In the following, the model is applied to the previously classified module types. The reader may refer to the Annexes for details. As for model accuracy (Annex A3), one estimates a maximum temperature error of ~3%, with respect to their real space-time behaviour. As already noticed, the optimal charging time is t≈τ. For both continuous and discrete behaviour appliances, then, a charge and energetic efficiency of $1\text{-}e^{-1}$≈63% is predicted (provided the module is not over-dimensioned).

As shown in Annex A3, the model uses a number of approximations. Conditions on the Fourier (F_o≥0.04) and NTU (NTU≥3) numbers must then be satisfied. The above-mentioned conditions translate into each module having to be tall enough. In fact, see Eq. (A3.12), NTU is proportional to h_c. On the other hand, Eq. (A3.3), Fo is proportional to h_c-2. The coefficient in the F_o condition is two orders of magnitude lower than in the NTU condition and so, as verified, the former dominates. Given the module energy size (E_0) and base radius (r_c), the previously developed equations fix its height. The modules then have to be over-dimensioned by f_d, so as to make them tall enough and respect the F_o and NTU conditions.

4. MODULES

The charging process merely allows a limited charge efficiency. On the other hand, the choice of a factor f_d>1 increases efficiency. In fact, the energy accumulated into a module is given by $\eta_c\cdot E_0$. If one increases the energy size by making the module taller by a factor f_d, one can pretend to have the same energy size with an increased charge efficiency. As noticed above, in this paper it is assumed that $t_{opt}\approx\tau$. Therefore, see the comments to Eq. (24), one has $\theta=1/f_d+\theta_f$ where, as shown in Appendix A5, θ_f is the non-dimensional time taken by fusion to occur. The charging efficiency for a non-upscaled module must then be multiplied by fd, to give the effective charging efficiency.

Based on these facts, it is then possible to give expressions for the module efficiency. In particular, see Annex A4, an expression valid for all the previously defined module categories is:

$$\tilde{T}_{\infty}=T_{\infty}-k_1\cdot(1-e^{-1})\cdot(T_{\infty}-T_0) \quad (37)$$

$$T=\tilde{T}_{\infty}+(T_0-\tilde{T}_{\infty})\cdot exp(-\theta) \quad (38)$$

$$\eta_c^{opt}=f_d\cdot(1-k_2\cdot exp(-\frac{1}{f_d})) \quad (39)$$

$$\eta_e^{opt}=f_d\cdot(1-exp(-\frac{1}{f_d})) \quad (40)$$

In the previous equations, k1 is 0, unless for VITSHMs and VITPCMs, in which case it is 1. k_2 is 1, unless for CITPCMs and VITPCMs, in which case it is 1/2.

5. APPROXIMATIONS

In Annex A4, it is shown that the previous equations are approximations to the exact formulae. Using these approximate formulae, however, leads to a conservative design choice (to slightly overestimating module height, which can only increase thermal exchange efficiency, given the previously mentioned NTU conditions). Based on the results in Annex A3, the model is expected to reproduce the experimental results within ~3%. In Annex A4, it is equally shown that, for VITSHMs and VITPCMs, the efficiency expressions should be multiplied by correction factors ~1, ignoring which leads to slightly overestimating module height, with beneficial effects on thermal exchange efficiency.

The expression for the PCM module charging time, in principle, should be modified by adding the fusion time to the set 18 min. On the other hand, Table 3 shows that the fusion heats of interest are <514 MJ/m^3. Furthermore, Tables 4-7 show that transferred power is larger than 84·0.8=67 W. The storage units have 5 mm diameter and height <20 cm. A fusion process duration <30 sec, therefore negligible, is then calculated.

6. RESULTS

The mathematical model was simulated by an Excel spreadsheet. Using the model developed here, optimal configurations for both fixed beds and shell-and-tube heat exchangers, loaded with spherical or cylindrical heat storage units (made up of suitable heat storage materials), were calculated. The storage modules have an energy size of 1.4 MJ, approximately corresponding to the energy needed for heating water in a dish-washer cycle [MOXOFF, 2013a]. As for the thermo-vector fluid, air, with a maximum flow rate of 6 l/s per module, was chosen, as determined by structural and acoustical considerations (water would require lower flows, which would not pass through the heat exchanger [Zavattoni et al., 2014].

A domestic kitchen heat storage module was considered, coupled to a thermal bus that connects a refrigerator, an induction cook-top plane and a domestic oven. For the refrigerator, one must have two parallel heat storage modules [Mukherjee et al., 2011], since while one module is charging, the other is in the discharge phase. For discrete behaviour appliances, instead, a single module suffices. The cook-top induction plane charge time is ~18 min [Zavattoni et al., 2014]. The domestic oven charge time can be determined at will (within technological limits) by choosing a suitable air extraction pump. In the case of a refrigerator, the charge time depends on how much energy must be accumulated. Envisaging possible synchronization among the appliances, a common charge time of 18 min was then chosen [MOXOFF, 2012a - MOXOFF, 2013b]. The appliances considered were:

- A refrigerator, dissipation temperature: 40°C, dissipated power: 84 W, charging time: 18 min, stored energy: 0.1 MJ, air flow rate: 4.0 l/s.
- An induction cook plane, dissipation temperature: 60°C, dissipated power: 100 W, charging time: 18 min, stored energy: 0.1 MJ, air flow rate: 2.4 l/s.
- An oven, equivalent dissipation temperature: 80°C, real dissipation temperature range (as time proceeds): 20-100°C, charging time: 18 min, stored energy: 1.1 MJ, dissipated power: 365 W, air flow rate: 5.9 l/s.

In Tables 4-7, results for cylindrical modules with 50 cm diameter are shown. As for efficiencies and volume, the smallest factor needed for satisfying model approximations was chosen and efficiencies were calculated accordingly (and turned out to be ~80-150%, since the effective efficiency, due to the way it is defined, can be >100%). In order to rank the various solutions, a figure of merit, the power density (up to ~200 W/kg), was devised:

$$\rho_p=\frac{E\cdot\eta_c}{\rho_m\cdot V_m\cdot t_{opt}} \quad (41)$$

As for shell-and-tube heat exchangers, the following solutions were found:

- ~50×50×25 cm, ~30 kg (PCMs),
- ~50×50×40 cm, ~110 kg (SHMs).

On the other hand, fixed beds turned out to be ~30% shorter and ~10% lighter. Since module height is not critical, and fixed beds are harder and more expensive to build, the choice of election is PCM-based shell-and-tube heat exchangers.

7. DISCUSSION

As shown in Annex A3, a maximum error of ~3% is predicted, with respect to the real temperature behaviour of the system. A priori, one might worry about pressure drop in the heat exchangers. However (Annex A7), the maximum pressure drop is <0.5% of the atmospheric pressure and can then be neglected. Let us finally notice that both the fixed bed and the shell-and-tube exchanger have to be equipped with baffles. Baffles have different functions [Mukherjee, 1998]: they contribute to the structural stability, drive the flow by avoiding blind corners, make the flow orthogonal to the axis, improving the heat exchange rate. Simulation results imposed to devise a mechanism for increasing the mean area velocity, so as to increase the system NTUs. Baffles turned out to be the answer.

The model described here was conceived in order to fulfill the request, by Whirlpool Europe, to dimension a green kitchen system for which, to the best of the author's knowledge, no model existed in the literature. Experimental tests were

performed by Whirlpool Europe [Zavattoni et al., 2014] but no details were released in the open literature. Our exercise was meant to obtain a proof-of-concept, so that Whirlpool might decide whether to build and experiment a prototype. To the best of our knowledge, however, no prototype was built, therefore our model, although its approximations were demonstrated to be reasonable, was not validated experimentally.

8. CONCLUSION

The model is based on a lumped parameter approach, which makes it sufficiently simple and manageable. As previously stated, and shown in Appendix A3, a maximum error of ~3% is predicted, with respect to the real behaviour of the system. The model, however, could not be validated experimentally. Unfortunately, not all the possible heat storage materials could be considered, due to inconsistencies in literature data. However, ~20 SHMs and PCMs were considered, representing all the available material typologies. We acknowledge the existence of thermoplastic materials [Oguzhan et al., 2019], for which, however, we could not find useful data.

Our simulations allowed us to find a PCM-based and a SHM-based configuration, satisfying our specifications with the largest exergetic efficiency, namely ~50x50x25 cm, ~30 kg (PCM) and ~50x50x40 cm, ~110 kg (SHM). The PCM-based module is more compact and less heavy, so we tend to prefer it. Starting from the results achieved, future work might involve numerical optimization of the best configurations, using CFD software. Needless to say, the model would need experimental validation, which at the moment is lacking. In any case, the efficiencies calculated with a lumped parameter model are a lower estimate of those calculated with a 2D model [Taylor et al., 1991a - Taylor et al., 1991b]; the model, consequently, produces a conservative design. An interesting development might be an extension of the model to restaurant or industrial kitchens, especially in connection with a financial analysis.

NOMENCLATURE

ρ_m : *Material density (kg.m^{-3})*
C : *Material specific heat (J.K^{-1}.kg^{-1})*
ΔT : *Fluid minus solid temperature (K)*
ρ_e : *Material energy density (J.m^{-3})*
ΔH : *Material fusion enthalpy (J)*
V_m : *Material volume (m^3)*
E_0 : *Module energy size (J)*
f_d : *Module volume factor (n.d.)*
ε_3 : *1-ε3 is 3D porosity (n.d.)*
ε_2 : *1-ε2 is 2D porosity (n.d.)*
V_c : *Module volume (m^3)*
h_c : *Module height (m)*
a_c : *Module shape factor (n.d.)*
a_u : *Module unit shape factor (n.d.)*
r_c : *Module radius (m)*
r_u : *Module unit radius (m)*
N_u : *Total number of units (n.d.)*
S_u : *Total heat exchange area (m^2)*
M : *Material mass (kg)*
$\dot{m}$: *Fluid mass flow rate (kg.s^{-1})*
C_p : *Fluid specific heat (J.K-1.kg-1)*
θ : *Non-dimensional time (n.d.)*
NTU : *Number of Thermal Units (n.d.)*
y : *NTU-derived non-dimensional parameter (n.d.)*
U : *Heat exchange coefficient (W.m^{-2}.K^{-1})*
T_0 : *Room temperature (K)*
T_{in} : *Inlet fluid temperature (K)*
T_∞ : *Asymptotic value of T_{in} (K)*
T_{opt} : *Optimal module charging temperature (K)*
t_{opt} : *Optimal module charging time (s)*
W : *Power transported by the fluid (W)*
Φ : *Fluid volume throughput (m^3.s^{-1})*
E : *Energy deposed in the material (J)*
Nu : *Nusselt number (n.d.)*
Pr : *Prandtl number (n.d.)*
Re : *Reynolds number (n.d.)*
k_f : *Fluid thermal conductivity (W.m^{-1}.K^{-1})*
k_m : *Material thermal conductivity (W.m^{-1}.K^{-1})*
μ_f : *Fluid viscosity (N.s.m^{-2})*
v_f : *Fluid mean velocity (m/s)*
f_p : *Baffle pitch over heat module diameter (n.d.)*
η_c : *Module charging efficiency (n.d.)*
η_e : *Module energetic efficiency (n.d.)*
η_c^{opt} : *Optimum module charging efficiency (n.d.)*
η_e^{opt} : *Optimum module energetic efficiency (n.d.)*
ρ_p : *Module power density (J.m^{-3})*
t : *Time coordinate (s)*
F_o : *Fourier number (n.d.)*
f_e : *Module energetic efficiency correction factor (n.d.)*
f_c : *Module charging efficiency correction factor (n.d.)*
W_{ex} : *Power exchanged between material and fluid (W)*
$LMTD$: *Log Mean Temperature Difference (K)*
S : *Heat exchange area (m^2)*
T_f : *Fluid outlet temperature (K)*
T_s : *Solid material temperature (K)*
W_f : *Heat exchanged between material and fluid (J)*
W_s : *Power exchanged between material and fluid (J)*
P : *Heat exchanger wetted perimeter (m)*
x : *Distance coordinate (m)*
λ : *Spatial temperature decay constant (m)*
$\tilde{T}_\infty$: *Effective oven dissipation temperature (K)*

t_c : Module charging time (s)
dm : Infinitesimal mass entering the oven (kg)
σ : Oven thermal disturbance standard deviation (m)
α_p : Air thermal diffusivity ($m2.s^{-1}$)
l_o : Oven characteristic length (m)
t_o : Oven thermal disturbance characteristic time (s)
Bi : Biot number (n.d.)
α_m : Material thermal diffusivity ($m^2.s^{-1}$)
t_u : Module unit heat diffusion time scale (s)
τ_u : Module unit thermal equilibrium time scale (s)
KR : Ratio between material and fluid thermal conductivities (n.d.)
ε_{fit} : Error due to temperature fitted by an exponential (K)
ε_{nct} : Error due to non-constant temperature (K)
ε_{dyn} : Error due to material lagging behind fluid (K)
ε : Total temperature error (K)
ΔT_m : Temperature drop across the material (K)
T_f : Material fusion temperature (K)
θ_f : Material fusion duration (τ depending on C_l) (s)
$\theta^{(l)}_f$: Material fusion ending time (τ depending on C_l) (s)
$\theta^{(s)}_f$: Material fusion ending time (τ depending on C_s) (s)
C_s : Material solid specific heat ($J.K^{-1}.kg^{-1}$)
C_l : Material liquid specific heat (J.K-1.kg-1)
C_a : Material average specific heat ($J.K^{-1}.kg^{-1}$)
C_f : Material fusion specific heat ($J.K^{-1}.kg^{-1}$)
C_t : Material total specific heat ($J.K^{-1}.kg^{-1}$)
ξ_s : Material solid non-dimensional specific heat (n.d.)
ξ_l : Material liquid non-dimensional specific heat (n.d.)
ξ_a : Material average non-dimensional specific heat (n.d.)
ξ_f material fusion non-dimensional specific heat (n.d.)
ξ_t : Material total non-dimensional specific heat (n.d.)
θ^{opt} : Optimum module charging time (τ depending on C_l) (s)
E : System exergy (J)
U : System internal energy (J)
p_0 : Environmental pressure (Pa)
V : System volume (m^3)
S system entropy ($J.K^{-1}$)
W : Work performed by the system (J)
ΔS_{tot} : System plus environment entropy variation (J.K-1)
W_{dis} : Dissipated work (J)
η_{ex} : Exergetic efficiency (n.d.)
W_{max} : Maximum work performed by the system (J)
τ_∞ : A non-dimensional temperature (n.d.)
$<\theta_{opt}>$: Average value of θ_{opt} (s)
α : A function of $<\theta_{opt}>$ (n.d.)
T_c : Temperature at which the modulus charges (K)
θ_c : Non-dimensional Tc (τ depending on C_l) (n.d.)
Δp_{fb} : Fluidized bed pressure drop (Pa)
d_u : Module unit diameter (m)
Δp_{hh} : Heat exchanger pressure drop (Pa)
N_b : Number of heat exchanger baffles (n.d.)
$\tilde{N}_r$: Effective number of heat exchanger tube rows (n.d.)
f : Friction factor (n.d.)
d_c : Module diameter (m)
v_{mf} : Minimal fluidization velocity ($m.s^{-1}$)
g : Gravitational acceleration ($m.s^{-2}$)

ACKNOWLEDGEMENTS

I express my gratitude to dr. Paolo Ferrandi, dr. Chiara Riccobene and dr. Matteo Longoni (MOXOFF) for their invaluable help. My gratitude, also, to prof. Alfio Quarteroni (Politecnico di Milano) and dr. Ottavio Crivaro (MOXOFF) for their constant encouragement and for allowing and supporting the publication of this paper. I also gratefully acknowledge the contribution of dr. John Doyle (Whirlpool Europe).

DATA AVAILABILITY STATEMENT

The published publication includes all graphics and data collected or developed during the study.

CONFLICT OF INTEREST

The author declared no potential conflicts of interest with respect to the research, authorship, and/or publication of this article.

ETHICS

There are no ethical issues with the publication of this manuscript.

FINANCIAL DISCLOSURE

The authors declared that this study has received no financial support.

REFERENCES

Ahmed, A., & Lebedev, V.A. (2018). Thermal energy storage by using latent heat storage materials. *International Journal of Scientific & Engineering Research, 9*(5), 1442–1447.

BDF Industries (2017). *Regenerative and Recuperative Furnace*. www.bdfindustriesgroup.com/products/melting-furnace-rigen.

Bejan, A. (1978). Two thermodynamic optima in the design of sensible heat units for energy storage. *ASME Journal of Heat Transfer, 100*(4), 708–712. [CrossRef]

Biyikoglu, A. (2002). Optimization of a sensible heat cascade energy storage by lumped model. *Energy Conversion and Management, 43*(5), 617–637. [CrossRef]

Bjurström, H., & Carlsson, B. (1985). An exergy analysis of sensible and latent heat storage. *Heat Recovery Systems, 5*(3), 233–250. [CrossRef]

Caillat, T., Fleurial, J.- P., Snyder, G. J., Zoltan, A., Zoltan, D., & Borshchevsky, A. (1999). A new high efficiency segmented thermoelectric unicouple.

34th Intersociety Energy Conversion Engineering Conference, 2567–2570. [CrossRef]

Carvill, J. (2003). *Mechanical Engineer's Data Handbook*. Butterworth Heinemann.

Chauk, S. S., & Fan, L. S. (1998). Heat Transfer in Packed and Fluidized Beds. In: Rohsenow, W.M., Hartnett, J.R., & Cho, Y.I. (Eds.), *Handbook of Heat Transfer* (pp. 13.1-13.45). McGraw-Hill.

Dincer, I., & Cengel, Y. A. (2001). Energy, entropy and exergy concepts and their roles in thermal engineering. *Entropy, 3*(3), 116–149. [CrossRef]

Dincer, I., Dost, S., & Li, X. (1997). Performance analysis of sensible heat storage systems for thermal applications. *International Journal of Energy Research, 21*(12), 1157–1171. [CrossRef]

Fernandez, A. I., Martínez M., Segarra M., Martorell I., & Cabeza L. F. (2010). Selection of materials with potential in sensible thermal energy storage. *Solar Energy Materials and Solar Cells, 94*(10), 1723–1729. [CrossRef]

Ganapathy, V. (2015). *Steam Generators and Waste Heat Boilers for Process and Plant Engineers*. www.brazedplate.com. [CrossRef]

Hales, T. C., & Ferguson, S. P. (2006). A formulation of the Kepler conjecture. *Discrete & Computational Geometry, 36*(1), 21–69. [CrossRef]

Holdich, R. G. (2002). *Fundamentals of particle technology*. Midland Information Technology and Publishing.

Hussam, J., Khordehgah, N., Almahmoud, S., Delpech, B., Chauhan, A., & Tassou, S. A. (2018). Waste heat recovery technologies and applications. *Thermal Science and Engineering Progress, 6*, 268–289. [CrossRef]

Institute for Industrial Productivity (2017). *Regenerative Burners for Reheating Furnaces*. www.ietd.iipnetwork.org/content/regenerative-burners-reheating-furnaces.

IPIECA (2022). *Heat Exchangers*. www.ipieca.org/resources/energy-efficiency-solutions/heat-exchangers-2022.

JHCSS (2017). *Heat Pipes*. www.jhcss.com.au/products-1/thermal-management/heat-pipes-heat-exchangers.

Mardiana-Idayua, A., & Riffat, S. B. (2012). Review on heat recovery technologies for building applications. *Renewable and Sustainable Energy Reviews, 16*(2), 1241–1255. [CrossRef]

Mehrer, A., & Stolwijk, A. (2009). Heroes and Highlights in the History of Diffusion. *Diffusion Fundamentals*, 11(1), 1–32.

MOXOFF (2012a). *Accumulo delle potenze perse: studio delle tecnologie adatte a un immagazzinamento delle potenze dagli elettrodomestici* [unpublished technical report 4.1.3]. MOXOFF.

MOXOFF (2012b). *Accumulo termico: evidenza del suo funzionamento attraverso la modellizzazione e la prototipazione virtuale* [unpublished technical report 4.1.4]. MOXOFF.

MOXOFF (2013a). *Riutilizzo della potenza termica in eccesso: analisi di letteratura e selezione delle tecnologie più promettenti* [unpublished technical report 4.1.5]. MOXOFF.

MOXOFF (2013b). *Riutilizzo della potenza termica in eccesso: selezione del sistema migliore e analisi dell'efficienza* [unpublished technical report 4.1.6]. MOXOFF.

Mukherjee, R. (1998). Effectively design shell-and-tube heat exchangers. *Chemical Engineering Progress, 94*(2), 21–37.

Mukherjee, R., Singh, D., Grewal, R., Ranjan, S., Olivani, A., Alshourbagy, M., & Pannock, J. (2011). *Assembly of domestic appliances with a system for utilizing waste heat from refrigerator in a washing appliance* [unpublished European patent application 11189489.5]. European Patent Office.

Oguzhan, D., Marengo, M., & Bertola, V. (2019). Thermal performance of pulsating heat stripes built with plastic materials. *Journal of Heat Transfer, 141*(9), 1–8. [CrossRef]

Rosen, M. A., Hooper, F.C., & Barbaris, L. N. (1988). Exergy analysis for the evaluation of the performance of closed thermal energy storage systems. *Journal of Solar Energy Engineering, 110*(4), 255–261. [CrossRef]

Sarbu, I., & Sebarchievici, C. (2018). A comprehensive review of thermal energy storage. *Sustainability, 10*(191), 1–32. [CrossRef]

Shah, R. K., & Sekulic, D. P. (1998). Heat Exchangers. In: Rohsenow, W.M., Hartnett, J.R., Cho, Y.I. (Eds.), *Handbook of Heat Transfer* (pp. 17.1–17.169), McGraw-Hill.

Sharma, A., Tyagi, V. V., Chen, C. R., & Buddhi, D. (2009). Review on thermal energy storage with phase change materials and applications. *Renewable and Sustainable Energy Reviews, 13*(2), 318–345. [CrossRef]

Sharma, S. D., & Sagara, K. (2005). Latent heat storage materials and systems: A review. *International Journal of Green Energy, 2*(1), 1–56. [CrossRef]

Song, C., Wang, P., & Makse, H. A. (2008). A phase diagram for jammed matter. *Nature, 453*(7195), 629–632. [CrossRef]

Spirax Sarco (2011). *Miscellaneous Boiler Types, Economizers and Superheaters*. www.spiraxsarco.com/learn-about-steam/the-boiler-house/miscellaneous-boiler-types-economisers-and-superheaters.

Stefanou, M. R. (2017). Performance evaluation of an ORC unit integrated to a waste heat recovery system in a steel mill. *IV International Seminar on ORC Power Systems*, 535–542. [CrossRef]

Taylor, M. J., Krane, R. J., & Parsons, J. R. (1991a). Second law optimization of a sensible heat thermal energy storage system with a distributed storage element - Part I. *ASME Journal of Energy Resources Technology, 113*(1), 20–26. [CrossRef]

Taylor, M. J., Krane, R. J., & Parsons, J. R. (1991b). Second law optimization of a sensible heat thermal energy storage system with a distributed storage element - Part II. *ASME Journal of Energy Resources Technology, 113*(1), 27–32. [CrossRef]

Thermtech (2014). *Reducing energy costs with economizers*, www.thermtech.co.uk/reducing-energy-costs-with-economisers.

Wall, G. (1977). *Exergy - A Useful Concept within Resource Accounting* [unpublished technical report 77-42]. Chalmers University of Technology.

Yodrak, L., Rittidech, S., Poomsa-ad, N., & Meena, P. (2010). Waste heat recovery by heat pipe air-preheater to energy thrift from the furnace in a hot forging process. *American Journal of Applied Sciences, 7*(5), 675–681.

Yovanovich, M.M. (1998). Conduction and Thermal Contact Resistances. In: Rohsenow, W.M., Hartnett, J.R., Cho, Y.I. (Eds.), *Handbook of Heat Transfer* (pp. 3.1–3.73), McGraw-Hill.

Zavattoni, S. (2012). *Household Appliances: Waste Heat Assessment and Thermal Energy Storage Options* [unpublished technical report]. SUPSI.

Zavattoni, S., Garcia-Polanco, N., Capablo, J., & Doyle, J. P. (2014). Packed bed latent heat TES for home appliance waste heat storage - System dimensioning and CFD analysis. *International Conference on Home Appliance Technologies*. Available from: www.iapp-greenkitchen.eu.

ANNEX A1
HEAT STORAGE SYSTEM MODEL

Let us generalize the model of a heat/storage recovery system to a time-variable inlet temperature profile. In particular, the analysis assumes that a hot fluid enters an insulated vessel, where it interacts with a sensible heat material (SHM), supposed to have constant temperature, and heats it. Thermal energy can then be stored. Let us then express W_{ex}, the power exchanged between the material and the thermo-vector fluid, by using the Log Mean Temperature Difference (LMTD) formalism [Bejan, 1978]:

$$W_{ex} = U \cdot S \cdot LMTD \quad \text{(A1.1)}$$

$$LTMD = \frac{T_{\text{in}}(t) - T_f}{log(\frac{T_{\text{in}}(t) - T_s}{T_f - T_s})} \quad \text{(A1.2)}$$

where U is the heat transfer coefficient, S is the heat exchange area, T_f is the fluid outlet temperature, T_{in} (t) is the fluid inlet temperature (supposed to be varying in time) and T_s is the solid temperature.

The exchanged power, as seen from the fluid side, is given by:

$$W_f = W_{\text{ex}} = \dot{m} \cdot C_p \cdot (T_{\text{in}} - T_f(t)) \quad \text{(A1.3)}$$

where $\dot{m}$ is the fluid flow rate, C_p is its specific heat. The exchanged power, as seen from the solid side, is given by:

$$W_s = W_{ex} = \frac{M \cdot C \cdot dT_s}{dt} \quad \text{(A1.4)}$$

where M is the solid mass, C the solid specific heat.

Combining Eqs. (A1.1)-(A1.3):

$$T_f = y \cdot T_s + (1 - y) \cdot T_{\text{in}}(t) \quad \text{(A1.5)}$$

where y is a parameter characterizing heat transfer in the system. As shown in Annex A3, y≈1 to any practical purpose.

In particular:

$$y = 1 - exp(-NTU) \quad \text{(A1.6)}$$

where the parameter NTU (Number of Transfer Units) is a non-dimensional number [Bejan, 1978]:

$$NTU = \frac{U \cdot S}{\dot{m} \cdot C_p} \quad \text{(A1.7)}$$

In Annex A3, it is shown that the condition NTU→∞ is imposed to the system, so that:

$$T_f = T_s \quad \text{(A1.8)}$$

By combining Eqs. (A1.3)-(A1.5), one has the following differential equation:

$$\frac{\tau}{y} \cdot \dot{T}_f = -T_f + T_{\text{in}}(t) + \tau \cdot (\frac{1}{y} - 1) \cdot \dot{T}_{\text{in}}(t) \quad \text{(A1.9)}$$

where τ is given by Eq. (A1.10) and T_{in} is variable in time (for physical reasons, at infinity it must flatten to T_∞). Both the inlet and outlet temperatures, at t=0, are supposed to be room temperature (T_0). Given these conditions, the solution of the differential equation is an exponential, with:

$$\tau = \frac{M \cdot C}{\dot{m} \cdot C_p} \quad \text{(A1.10)}$$

where the coefficients added to the exponential and multiplying it are functions of time:

$$T_f = T_\infty + (T_0 - T_\infty) \cdot exp(-y \cdot \theta) + \Delta T_f(t) \quad \text{(A1.11)}$$

$$\Delta T_f(t) = exp(-y \cdot \theta) \cdot \int_0^{y \cdot \theta} ds \cdot exp(s) \cdot (\Delta T_\infty(s) + \tau \cdot (\frac{1}{y} - 1) \cdot \dot{T}_{\text{in}}(s)) \quad \text{(A1.12)}$$

and:

$$\Delta T_\infty(t) = T_{\text{in}}(t) - T_\infty \quad \text{(A1.13)}$$

As for the solid, by combining Eqs. (A1.3) to (A1.5), one has:

$$\frac{\tau}{y} \cdot \dot{T}_s = -T_s + T_{\text{in}}(t) \quad \text{(A1.14)}$$

where the same fluid temperature hypotheses as above are assumed. In particular:

$$T_s = T_\infty + (T_0 - T_\infty) \cdot exp(-y \cdot \theta) + \Delta T_s(t) \quad \text{(A1.15)}$$

$$\Delta T_s(t) = exp(-y \cdot \theta) \cdot \int_0^{y \cdot \theta} ds \cdot exp(s) \cdot \Delta T_\infty(s) \quad \text{(A1.16)}$$

These solutions can be unified and simplified under hypothesis that NTU→∞:

$$T = T_\infty + (T_0 - T_\infty) \cdot exp(-\theta) + \Delta T(t) \quad \text{(A1.17)}$$

$$\Delta T(t) = exp(-\theta) \cdot \int_0^{\theta} ds \cdot exp(s) \cdot \Delta T_\infty(s) \quad \text{(A1.18)}$$

$$\Delta T_\infty(t) = T_{\text{in}}(t) - T_\infty \quad \text{(A1.19)}$$

In the previous equations, T is the common temperature to the outlet fluid and solid. Of special interest is the case NTU→∞ and $T_{in}(t)=T_\infty$ (constant inlet temperature):

$$T = T_\infty + (T_0 - T_\infty) \cdot exp(-\theta) \quad \text{(A1.20)}$$

For any practical purpose, the previous equation is applicable to all the systems described here. In the previous equations, the non-dimensional time is defined as:

$$\theta = \frac{t}{\tau} \quad \text{(A1.21)}$$

Finally, let us calculate the temperature distribution inside the exchanger:

$$dW_{ex} = U \cdot (T_f - T_s) \cdot P \cdot dx \quad \text{(A1.22)}$$

$$dW_f = dW_{ex} = -\dot{m} \cdot C_p \cdot \partial_x(T_f - T_s) \cdot dx \quad \text{(A1.23)}$$

where P is the wetted perimeter:

$$\partial_x(T_f - T_s) = -(T_f - T_s)/\lambda \quad \text{(A1.24)}$$

where h_c is the cylindrical module height. In the previous equation:

$$\lambda = \frac{h_c}{NTU} \tag{A1.25}$$

According to the boundary conditions, at x=0 the fluid temperature must be T_∞ at any time. The fluid temperature at x=h_c must be established, at any time, by Eq. (A1.20) or its various generalizations. In this case, Eq. (1.24) gives:

$$T_f(x,t) = T_\infty + (T - T_\infty) \cdot \frac{(1-\exp(-\frac{x}{\lambda}))}{(1-\exp(-\frac{h_c}{\lambda}))} \tag{A1.26}$$

Alternatively, provided Eq. (A1.20) holds, the temperature profile is:

$$T_f(x,t) = T_\infty + (T_0 - T_\infty) \cdot exp(-\frac{t}{\tau}) \cdot \frac{(1-exp(-\frac{x}{\lambda}))}{(1-exp(-\frac{h_c}{\lambda}))} \tag{A1.27}$$

According to Eqs. (A1.26) and (A1.27) if, as in our configurations, one has NTU>>1, then λ→0 and the fluid temperature is nearly constant inside the exchanger. Finally, it has to be noticed that the previous calculations are valid for cylindrical units. However, under the hypothesis that the spherical units are piled up in cylinders with base diameter equal to their diameter, it is easy to show that the previous calculation are still valid, as long as h_c is replaced by:

$$\frac{4}{3} \cdot h_c \tag{A1.28}$$

ANNEX A2
DOMESTIC OVEN MODEL

Let us develop a mathematical model for a heat storage/recovery system, coupled to a domestic oven. Later it will be shown that the temperature of an oven whose thermal energy in excess of T_0 is removed by sucking hot air from its cavity and replacing it with cold air is given by:

$$T_{\text{in}}(t) = T_\infty + (T_0 - T_\infty) \cdot exp(-\theta) \tag{A2.1}$$

By combining Eqs. (A1.17)-(A1.19) with Eq. (A2.1), one has, for the fluid and solid outlet temperature:

$$T = T_0 + (T_\infty - T_0) \cdot \theta \cdot exp(-\theta) \tag{A2.2}$$

Inspection of the previous equation shows that it only makes sense to charge the module until θ=1. Beyond this time, in fact, the material would be giving heat to the thermo-vector fluid. One would also like to have:

$$E = M \cdot C \cdot \Delta T \tag{A2.3}$$

$$W = \dot{m} \cdot C_p \cdot \Delta T \tag{A2.4}$$

where E is the energy deposed in the module, W is the average power transported by the fluid, ΔT is a suitable temperature difference. Considering the situation at θ=1 and using Eqs. (A2.1) and (A2.2), one shows that Eqs. (A2.3) and (A2.4) apply, with:

$$\Delta T = \widetilde{T_\infty} - T_0 \tag{A2.5}$$

where $\widetilde{T_\infty}$ is the temperature at θ=1. One then has:

$$\widetilde{T_\infty} = T_\infty - k \cdot (T_\infty - T_0) \tag{A2.6}$$

$$k = 1 - e^{-1} \approx 0.63 \tag{A2.7}$$

In the previous equations:

$$\theta = \frac{t}{\tau} \tag{A2.8}$$

$$\tau = \frac{M \cdot C}{\dot{m} \cdot C_p} \tag{A2.9}$$

where M is the solid mass, C the solid specific heat, C_p the fluid specific heat, $\dot{m}$ the fluid flow rate.

It is possible to prove that the monotonically increasing part of Eq. (A2.2) can be approximated by an exponential rise, having an effective asymptotic temperature given by Eqs. (A2.6) and (A2.7). In order to demonstrate this, let us first observe that the above-mentioned curve portion can be fitted by:

$$T = \widetilde{T_\infty} + (T_0 - \widetilde{T_\infty}) \cdot exp(-e \cdot \theta) \tag{A2.10}$$

In fact, if one tries to fit Eq. (A2.2) with Eq. (A2.10), with a time constant:

$$\theta' = a \cdot \theta \tag{A2.11}$$

it turns out that:

$$\theta \cdot exp(-\theta) \approx (1-k) \cdot (1 - exp(-a \cdot \theta)) \tag{A2.12}$$

and, taking the limit for θ → 0:

$$a = \frac{1}{1-k} = e \approx 2.72 \tag{A2.13}$$

The previous results are suggested by the physics of the problem. They were double-checked through a least square fit, performed with Mathematica, by sampling the function on 10^5 equally spaced points. The result was:

$$\begin{aligned} k &\approx 0.59 \\ a &\approx 2.67 \end{aligned} \tag{A2.14}$$

The parameter values suggested by the physics of the problem were adopted, so that:

$$\begin{aligned} k &= 1 - \frac{1}{e} \approx 0.63 \\ a &= e \approx 2.72 \end{aligned} \tag{A2.15}$$

By employing Mathematica, a fitting error of 1.3%, with T_∞=180 °C, T_0=20 °C, was calculated. These are the typical temperatures for a domestic oven [R. Mereu, personal communication, 2013] and the effective temperature, then, turned out to be ~80 °C. Due to error propagation, correction factors are needed for the charge and energy efficiencies of the system, with respect to the expressions coming from Eq. (A2.10). Such correction factors were calculated with Mathematica and:

$$\eta_c = (1 - exp(-\theta')) \cdot (1 + 0.37 \cdot \theta - 0.30 \cdot \theta^2) \tag{A2.16}$$

and:

$$\eta_e = \frac{(1-exp(-\theta\prime))}{\theta\prime} \cdot (1 + 0.70 \cdot \theta) \quad \text{(A2.17)}$$

$$\theta' = e \cdot \theta \quad \text{(A2.18)}$$

Let us now give an expression for the module charging time, t_c. In this respect, let us observe that Eq. (A2.10) can be rewritten as:

$$T = \widetilde{T_\infty} + (T_0 - \widetilde{T_\infty}) \cdot exp(-\frac{t}{t_c}) \quad \text{(A2.19)}$$

with, see Eqs. (A2.3) and (A2.4):

$$t_c = \frac{E}{e \cdot W} \quad \text{(A2.20)}$$

Let us finally give a proof of the validity of Eq. (A2.1). The first question one might ask is how much thermal energy can be extracted from the hot air in the oven chamber and how much from its metallic structure. It was estimated [R. Mereu, personal communication, 2013] that ~1.1 MJ can be extracted by cooling the oven structure. On the other hand, cooling a 48 l (40x40x30 cm) chamber (from 180 to 20 °C), one can merely extract ~0.01 MJ (if one assumes, for air, a density of 1.2 kg/m^3 and a specific heat of 1 kJ/(kg·°C) [Carvill, 2003].

The model to be used for describing the oven structure cooling is the same as the one developed in Annex A1. Eq. (A2.1) therefore applies, provided the approximations used to derive it are applicable. It only remains to be checked that the characteristic time for making the oven structure temperature uniform is much smaller than the time-scale involved (18 min). Let us then observe that [Mehrer et al., 2009] a temperature disturbance spreads as a Gaussian, having a standard deviation:

$$\sigma(t) = \sqrt{2 \cdot \alpha_p \cdot t} \quad \text{(A2.21)}$$

where α_p is the thermal diffusivity. If one then supposes that such a temperature disturbance reaches the whole oven when $3 \cdot \sigma = l_o$, where l_o is its characteristic length, the time t_o at which this happens is:

$$t_o = \frac{l_o^2}{18 \cdot \alpha_p} \quad \text{(A2.22)}$$

Applying Eq. (A2.22) with αp=4.10-6 m^2/s (for a typical steel [Carvill, 2003]) and supposing that the structure is cooled by air from both its inner and outer sides so that, if the structure characteristic dimension is ~10 cm, then $l_0 \approx 5$ cm, the time-scale for heat diffusion turns out to be ~35 sec. Since one imposes a heat extraction time of 18 min, the characteristic time for uniforming temperature in the chamber is ~3% of the heat extraction time. One can then assume a uniform temperature distribution in the oven structure, as required by the approximations described in Annex A3.

ANNEX A3
MODEL APPROXIMATIONS

In Annex A1, two approximations were tacitly introduced:

- The material is able to follow the fluid time dynamics,
- The temperature of the material is constant through it.

As shown below, it turns out that these hypotheses can be translated into conditions on two non-dimensional numbers (Fo and NTU). In order to quantify the errors due to these approximations, let us define the Biot number (a non-dimensional radius) [Yovanovich, 1998]:

$$Bi = \frac{U \cdot r_u}{k_m} \quad \text{(A3.1)}$$

where U is the heat transfer coefficient, r_u is the storage unit radius, k_m is the material thermal conductivity. The heat storage unit can be considered as a point-like object if the Biot number is [Yovanovich, 1998]:

$$Bi < 0.20 \quad \text{(A3.2)}$$

but the discussion that follows shows that, for the systems proposed here, Bi≈0.45. The proposed lumped parameter approach would then seem not to be applicable. However, in the following it will be shown that condition (A3.2), in this case, is too drastic. The lumped parameter formalism indeed makes sense, provided the errors committed by applying it are kept under control.

In order to deal with axial diffusion, let us then introduce the Fourier number [Yovanovich, 1998]:

$$Fo = \frac{\alpha_m \cdot t}{h_c^2} \quad \text{(A3.3)}$$

where α_m is the thermal diffusivity of the material, t is a suitable time, h_c the module height and let us suppose that a heat wave starts from both sides of the cylinder, traveling towards its interior.

It is well-known [Mehrer et al., 2009] that the wave spreads as a Gaussian, with:

$$\sigma(t) = \sqrt{2 \cdot \alpha_m \cdot t} \quad \text{(A3.4)}$$

It can then be assumed that the temperature disturbance has reached the whole cylinder when $3 \cdot \sigma = \frac{1}{2} \cdot h_c$. This happens at a time:

$$t_u = \frac{h_c^2}{72 \cdot \alpha_m} \quad \text{(A3.5)}$$

In the following, it will be required that, although the body cannot be considered as a point-like object, the material and dimensions of the cylindrical units are such that the heat diffusion time-scale (as expressed by the Fourier number) is negligible with respect to the characteristic module cooling time.

In particular, in Annex A1 it is shown that the storage units get heated exponentially, with:

$$\tau = \frac{M \cdot C}{\dot{m} \cdot C_p} \quad \text{(A3.6)}$$

where M is the material mass, C the material specific heat, $\dot{m}$ the mass flow rate, Cp the fluid specific heat. It was then imposed that:

$$t_u \leq \frac{\tau}{3} \tag{A3.7}$$

(where the factor 3 is due to the exponential nature of the process) from which, by employing Eq. (A3.3) and (A3.5), it follows that:

$$Fo(\tau) \geq 0.04 \tag{A3.8}$$

Let us come to radial diffusion. In this respect, it can be noticed that if Eq. (A3.8) is satisfied for axial heat diffusion, it is satisfied for radial diffusion, as well, since in the cylindrical heat storage units one has $r_u<h_c$. However, there is one more condition to be satisfied. As previously mentioned, in fact, a lumped parameter solution is unacceptable for Bi>0.20. Nevertheless, such a solution can be employed if (as when justifying approximations) accuracy is not an issue [Yovanovich, 1998]. By using the lumped parameter solution, it can be shown that the heat storage unit reaches radial thermal equilibrium after [Yovanovich, 1998]:

$$\tau_u \approx \frac{1}{Bi} \cdot \frac{r_u^2}{\alpha_m} \tag{A3.9}$$

The material is then able to follow the time dynamics of the fluid if its time dynamics is fast enough, as compared to the thermal module time scale:

$$\tau_u \ll \tau \tag{A3.10}$$

It is easy to show that the previous equation can be rewritten as [Bejan, 1978]:

$$NTU \gg 1 \tag{A3.11}$$

and:

$$NTU = \frac{U \cdot S}{\dot{m} \cdot C_p} \tag{A3.12}$$

where U is the heat exchange coefficient, S is the heat exchange surface. Let us point out that Eq. (A3.11) is arrived at by employing, Eq. (A3.9), the definition [Yovanovich, 1998]:

$$\alpha_m = \frac{k_m}{\rho_m \cdot C} \tag{A3.13}$$

(where ρ_m is the material density) and Eqs. (A3.2) and (A3.6) for the Biot number and time constant.

Let us observe that conditions (A3.10) and (A3.11) are equivalent and the latter involves the NTU parameter. On the other hand, NTU depends on the exchange surface rather than on cylinder dimensions separately. The radial condition, then, applies to axial heat diffusion, as well.

One then can guarantee that the material is able to follow the time dynamics of the fluid by imposing Eq. (A3.8) and:

$$NTU \geq 3 \tag{A3.14}$$

where the condition given by Eq. (A3.14) is imposed since the parameter enters the error equations under an exponential. This gives an acceptable error, as shown later.

Let us finally evaluate the temperature errors related to model approximations. In particular, one has the following error sources:

- the temperature time-profile is just fitted by an exponential and not exponential (ε_{fit}),
- the temperature is not constant throughout the material (ε_{nct}),
- the material is not able to follow the fluid time dynamics (ε_{dyn}).

Temperature errors, here, are meant to be infinite-norm errors, i.e. maximum errors over the space and time domains, with respect to the real behaviour. The total model error was estimated by summing the various error terms in quadrature:

$$\epsilon = \sqrt{\epsilon_{fit}^2 + \epsilon_{nct}^2 + \epsilon_{dyn}^2} \tag{A3.15}$$

Let us first estimate the error due to fitting the oven temperature profile, Annex A2. The value of ε_{fit} is, of course, null for constant inlet temperature. Its value for a domestic oven was estimated, with Mathematica, to be 1.3%. Let us then estimate ε_{nct}. The temperature drop across the material ΔT_m can be calculated from W (the power transferred to the material), ΔT (the difference between the fluid inlet and room temperatures), η_e (the energy efficiency). In particular [Sharma et al., 2009]:

$$\Delta T_m \approx \frac{W}{U \cdot S} = \frac{\dot{m} \cdot C_p \cdot \Delta T \cdot \eta_e}{U \cdot S} = \frac{\Delta T \cdot \eta_e}{NTU} \tag{A3.16}$$

Let us assume $\varepsilon_{nct} \approx \frac{1}{2} \cdot \Delta T_m / T_\infty$ where T_∞ approximates the average temperature in the material, as shown by integrating Eq. (A1.27) with NTU->∞ (in practice, NTU≥3). One can then estimate the error.

In particular, one has:

$$\epsilon_{nct} \approx \frac{\Delta T \cdot \eta_e}{2 \cdot NTU \cdot T_\infty} \tag{A3.17}$$

By assuming $\Delta T \leq 60$ °C, $\eta_e \leq 0.9$, NTU=3 and $T_\infty \geq 40$ °C (313 °K) [MOXOFF, 2012b], one has ε_{nct}=2.9%. Let us then estimate εdyn, the error committed by having a finite NTU or, equivalently, y≠1. This is due to the fact that the material is not fully able to follow the fluid temperature variation. By using Eq. (A1.11), ε_{dyn} can be estimated by calculating dT/dy, then multiplying by dy≈1-y ($dy \approx e^{-NTU}$) and dividing by the average temperature:

$$\epsilon_{dyn}(t) = \frac{\Delta T}{T_\infty} \cdot (y \cdot \theta) \cdot exp(-y \cdot \theta) \cdot \frac{exp(-NTU)}{1 - exp(-NTU)} \tag{A3.18}$$

The previous expression reaches its maximum for $y \cdot \theta = 1$. For NTU>>1:

$$\epsilon_{dyn} \approx \frac{\Delta T}{T_\infty} \cdot exp(-(1 + NTU)) \tag{A3.19}$$

By assuming that NTU=3, $\Delta T \leq 60$ °C, $T_\infty \geq 40$ °C (313 °K) [MOXOFF, 2012b], one obtains ε_{nct}=0.4%.

By applying the above-mentioned equations, it is then possible to estimate the maximum space/time error, with

respect to the real behaviour. In particular, by combining the previous results one can estimate that ε=3.2% for appliances dissipating at a time-variable temperature (ovens) and ε=2.9% for appliances dissipating at a time-constant temperature (refrigerators and cook-top planes). Given the approximate nature of the previous considerations, one can then state that the error is ~3% for any appliance type.

ANNEX A4
MODEL EXTENSION TO PCMS

Let us now extend the previous model to PCMs (phase change materials), as opposed to SHMs (sensible heat materials). For the fluid outlet and solid temperature (in the paper, it was shown that they nearly coincide), one has:

$$T = T_\infty + (T_0 - T_\infty) \cdot exp(-\theta) \quad \text{(A4.1)}$$

The previous equation holds for $T<T_f$, where T_f is the fusion temperature. During PCM fusion, one has:

$$T = T_f \quad \text{(A4.2)}$$

and, after fusion:

$$T = T_\infty + (T_f - T_\infty) \cdot exp(-(\theta - \theta_f - \theta_f^{(l)})) \quad \text{(A4.3)}$$

where θ_f is the time taken for fusion (normalized to the solid specific heat), $\theta^{(l/s)}_f$ is the fusion ending time (normalized to the liquid/solid specific heat). θ is also normalized to the liquid time constant. One then has to modify the SHM efficiency formulae accordingly. In order to achieve this, let us introduce an average specific heat:

$$C_a = \frac{C_s \cdot T_f - T_0}{T_\infty - T_0} + \frac{C_l \cdot T_\infty - T_f}{T_\infty - T_0} \quad \text{(A4.4)}$$

where C_s is the specific heat of the material in the solid state and C_l its specific heat in the liquid state. Let us notice that, provided $C_s \approx C_l$:

$$C_a \approx C_s \approx C_l \quad \text{(A4.5)}$$

One also has to introduce an effective specific heat that takes fusion into account:

$$C_e = C_a + C_f \quad \text{(A4.6)}$$

and:

$$C_f = \frac{\Delta H}{T_\infty - T_0} \quad \text{(A4.7)}$$

where C_f is the fusion equivalent specific heat and ΔH is the fusion enthalpy. The charge efficiency is then given by:

$$\eta_c = \frac{C_s \cdot (T_f - T_0) + \Delta H + C_l \cdot (T - T_f)}{C_e \cdot (T_\infty - T_0)} \quad \text{(A4.8)}$$

$$\eta_c = 1 - \xi_l \cdot exp(+\theta_f + \theta_f^{(l)} - \theta_f^{(s)}) \cdot exp(-\theta) \quad \text{(A4.9)}$$

The previous expression is obtained since, as shown by Eq. (A1.20):

$$\frac{T_\infty - T_f}{T_\infty - T_0} = exp(-\theta_f^{(s)}) \quad \text{(A4.10)}$$

In the previous equations, the following definition was employed:

$$\xi_i = \frac{C_i}{C_e} \quad \text{(A4.11)}$$

where i=a,s,l,f and:

$$\xi_a + \xi_t = 1 \quad \text{(A4.12)}$$

Under hypothesis (A4.5), then:

$$\eta_c = 1 - (1 - \xi_f) \cdot exp(+\theta_f) \cdot exp(-\theta) \quad \text{(A4.13)}$$

As for the energy efficiency, by repeating the steps leading to Eq. (A4.9):

$$\eta_e = \frac{1 - \xi_l \cdot exp(+\theta_f + \theta_f^{(l)} - \theta_f^{(s)}) \cdot exp(-\theta)}{\xi_l \cdot \theta} \quad \text{(A4.14)}$$

Under hypothesis (A4.5):

$$\eta_e = \frac{1 - (1 - \xi_f) \cdot exp(+\theta_f) \cdot exp(-\theta)}{(1 - \xi_f) \cdot \theta} \quad \text{(A4.15)}$$

Later in this Annex, it will be demonstrated that over-dimensioning the modules by a factor fd, so as to make the effective charge efficiency larger and allow modules to respect the conditions derived in Annex A3, is a convenient choice. The charge time is then $\tau \approx 1/f_d$, to which the fusion duration must be added. From now on, hypothesis (A4.5) will be adopted and the fusion duration (normalized to the liquid time constant) will be taken as

$$\theta_f = \frac{M \cdot \Delta H}{\eta_e^{opt} \cdot W \cdot \tau} = \frac{M \cdot \Delta H}{\eta_e^{opt} \cdot \dot{m} \cdot C_p \cdot \Delta T \cdot \tau} = \frac{\xi_f}{1 - \xi_f} \cdot \frac{1}{\eta_e^{opt}} \quad \text{(A4.16)}$$

where M is the material mass, ΔH the fusion enthalpy, W is the power transported by the fluid, C_p is the fluid specific heat, $\Delta T = T_\infty - T_0$. The optimum charge time is then given by:

$$\theta_{opt} = \frac{\xi_f}{1 - \xi_f} \cdot \frac{1}{\eta_e^{opt}} + \frac{1}{f_d} \quad \text{(A4.17)}$$

In the previous equation, the factor $1/f_d$ is due to the fact that τ is proportional to M, Eq. (A1.10), and the optimum charging time is calculated for a material mass M/fd, the mass the material would have, were the module not over-dimensioned.

Choosing $f_d>1$ increases efficiency. In fact, the energy accumulated into a module is $\eta_c \cdot E_0$. If one increases the energy size and makes the module larger by f_d, one can pretend to have the same energy size and an increased charge efficiency. Let us calculate the optimal charge efficiency. This quantity is obtained by multiplying Eq. (A4.13) by f_d and then employing Eq. (A4.16) and (A4.17):

$$\eta_c^{opt} = f_d \cdot (1 - (1 - \xi_f) \cdot exp(-\frac{1}{f_d})) \quad \text{(A4.18)}$$

The optimal system energy efficiency is then calculated by substituting Eq. (A4.16) and (A4.17) in Eq. (A4.15):

$$\eta_e^{opt} = \frac{\eta_c^{opt}}{f_d \cdot (1-\xi_f) \cdot \theta_{opt}} = f_d \cdot (1 - exp(-\frac{1}{f_d})) \quad \text{(A4.19)}$$

Let us point out that the PCMs considered in this study are such that, at ~10%:

$$\xi_l \approx \xi_s \approx \xi_f \approx \xi_a \approx \frac{1}{2} \quad \text{(A4.20)}$$

It was verified that, by using such an approximation, a conservative design criterion is actually employed, in that the module height is only slightly over-estimated (which can only increase the heat exchange efficiency). Finally, let us notice that the charge efficiency formulae for SMSs can be obtained by assuming a null value for ξ_f in Eqs. (A4.18) and (A4.19). This justifies Eqs. (37) to (40) of the main text.

ANNEX A5
EXERGETIC EFFICIENCY

Eq. (A1.20) shows that for t→∞ the fluid inlet temperature is equal to its outlet temperature. As a consequence of this, Annex A1, the charge efficiency tends to one but the energy efficiency tends to zero, since the only thing that the fluid does, for t→∞, is dissipating energy without transferring heat to the material. It is then intuitive that there must be an optimum point, beyond which it makes little sense to keep charging the heat storage module. In order to determine such a point, one has to calculate (and maximize) the exergetic efficiency of the system, i.e. the ratio between the potential work that is dissipated by the system and the maximum work the system can do while approaching equilibrium with its environment. This potential work has been named exergy [Wall, 1977].

The exergy of a system is:

$$E = U + p_o \cdot V - T_0 \cdot S \quad \text{(A5.1)}$$

where U is the internal energy of the system, T_0 is the environment temperature, p_0 is its pressure, V is the system volume, S is the system entropy. It is important to notice that Eq. (A5.1), by employing the first principle of thermodynamics, can be written as:

$$E = (p_o - p) \cdot V - (T_0 - T) \cdot S \quad \text{(A5.2)}$$

This shows that the exergy of a system in equilibrium with its environment is zero.

The importance of the exergy concept can be fully appreciated by observing that, if W is the work performed by the system, one has [Wall, 1977]:

$$W = E - T_0 \cdot \Delta S_{tot} \quad \text{(A5.3)}$$

where ΔS_{tot} is the total (i.e. system plus environment) entropy variation. Since the total entropy variation can only be positive (or null for reversible processes), Eq. (A5.3) leads to:

$$W \leq E \quad \text{(A5.4)}$$

An immediate consequence of Eq. (A5.3) is that the dissipated potential work is:

$$W_{dis} = T_0 \cdot \Delta S_{tot} \quad \text{(A5.5)}$$

The exergetic efficiency is then [Oguzhan et al., 2019 - Rosen et al., 1988]:

$$\eta_{ex} = \frac{W}{W_{max}} = \frac{E - W_{dis}}{E} = 1 - \frac{W_{dis}}{E} \quad \text{(A5.6)}$$

where W_{max}=E, Eq. (A5.4). For calculating this quantity, one has to determine:

$$\frac{W_{dis}}{E} \quad \text{(A5.7)}$$

Let us then start with appliances dissipating at a constant temperature, under y→1 (see Annex A1), and look at W_{dis} and the entropy variation ΔS_{tot}. The entropy variation includes [Bejan, 1978 - Rosen et al., 1988]:

- the fluid going from temperature T_∞ to T_0, at constant pressure,
- the environment receiving heat at temperature T_0, coming from the internal energy of the fluid (from T to T_0),
- the material going from temperature T_0 to temperature T.

It was verified that fusion, if present, gives a negligible contribution to W_{dis}. By using Eq. (A5.5), then, one has [Bejan, 1978]:

$$\frac{W_{dis}}{T_0} = -\dot{m} \cdot c_p \cdot t \cdot log(\frac{T_\infty}{T_0}) + \dot{m} \cdot c_p \cdot (\int_0^t ds \cdot (\frac{T - T_0}{T_0}) + M \cdot C \cdot log(\frac{T}{T_0}) \quad \text{(A5.8)}$$

where $\dot{m}$ is the fluid mass flow rate, C_p its specific heat, M the material mass, C its specific heat. As for exergy, one has to use of Eq. (A5.1), considering that the system that does work is the (non-expanding) fluid while it passes T to T_0.

By calculating E with reference to the (p_0,T_0) state one has [Bejan, 1978]:

$$\frac{E}{T_0} = \dot{m} \cdot c_p \cdot t \cdot (\frac{T_\infty - T_0}{T_0} - log(\frac{T_\infty}{T_0})) \quad \text{(A5.9)}$$

Let us then introduce the non-dimensional time and temperature [Bejan, 1978]:

$$\theta = \frac{\dot{m} \cdot c_p \cdot t}{M \cdot C} \quad \text{(A5.10)}$$

and:

$$\tau_\infty = \frac{T_\infty - T_0}{T_0} \quad \text{(A5.11)}$$

The exergetic efficiency, by using Eqs. (A1.7), (A1.20) and (A1.21), can then be expressed in the following way [Bejan, 1978]:

$$\eta_{ex} = \frac{1}{\theta \cdot (\tau_\infty - log(1+\tau_\infty))} \cdot (\tau_\infty \cdot (1 - exp(-\theta)) - log(1 + \tau_\infty \cdot (1 - exp(-\theta)))) \quad \text{(A5.12)}$$

This is the function to be maximized. In particular, for a given $\tau\infty$ (a given appliance at room temperature), one has to find a non-dimensional time θ_{opt} that maximizes the exergetic efficiency. This is the time beyond which there is no point in charging a module. As for the case of non-constant appliance inlet temperatures, e.g. a domestic oven, in Annex A2 it was shown that these appliances can be treated as if they dissipated heat at an effective constant temperature. Eq. (A5.12) can then be applied. As for systems with y≠1, Eq. (5.12) still applies, provided θ is just replaced by y·θ [Bejan, 1978]. Finally, let us notice that the optimum system exergetic efficiency is only a weak function of the appliance temperature. Its value turned out to be ~40%, for any appliance type and temperature.

ANNEX A6
SYSTEM OPTIMIZATION

To the best of the author's knowledge, according the thermal engineering literature [Bejan, 1978 - Bjurström et al., 1985] the thermodynamic optimization of a heat storage/recovery system cannot be performed analytically. In this Annex, it is demonstrated that a semi-analytical optimization can indeed be performed and, as a matter of fact, gives surprisingly simple results.

The thermodynamic module optimization was performed with Mathematica and turned out to be a lengthy exercise. Due to space limitations, here it is only possible to summarize the optimization steps. The author, upon request, can supply further details and the Mathematica script employed. The semi-analytical optimization process included the following steps:

- the derivative (FD) of the exergetic efficiency with respect to θ, fixing room temperature (RT) at 20 °C, was calculated,
- FD was developed in a Taylor series in τ_∞ and θ_{opt}, around their mean values,
- the mean value of τ_∞ was estimated as the τ_∞ at the mean value of the appliance dissipation temperature range (70 °C [MOXOFF, 2012b]),
- the mean value of θ_{opt} was estimated by graphically determining the θ for which the exergetic efficiency was maximum at 70 °C,
- the equation FD=0 was solved by series, replacing FD with its Taylor approximation at increasing τ_∞ and θ_{opt} orders,
- for each order, the values of FD on a suitable space-time grid were plotted. The minimum τ_∞ and θ_{opt} orders for which FD saturate were taken to represent the real solution,
- θ_{opt} and T_{opt}, were calculated as the analytical solution to the equation FD=0, as determined by Mathematica,
- ·rather than redoing the calculations for RT≠20 °C, it was verified that, for -40 °C<RT<40 °C, the solution varies by less than 1 °C.

The solution for the optimum module charge temperature, T_{opt}, obtained with the above-mentioned method, is:

$$T_{opt} = 0.70 \cdot T_\infty + 0.30 \cdot T_0 \quad \text{(A6.1)}$$

The fact that the coefficients of the polynomial add up to one was explained with the analytical developments that follow. In particular, it was found that the same results as the above-mentioned Taylor approach can be arrived at with simple analytical considerations. In fact, from Eq. (A1.20):

$$\theta_{opt} = log(\frac{T_\infty - T_0}{T_\infty - T_{opt}}) \quad \text{(A6.2)}$$

If one replaces the adimensional temperature θ_{opt} with its average value $<\theta_{opt}>$, the following expression is obtained:

$$T_{opt} = (1-\alpha) \cdot T_\infty + \alpha \cdot T_0 \quad \text{(A6.3)}$$

$$\alpha = exp(-<\theta_{opt}>) \quad \text{(A6.4)}$$

Besides re-deriving Eq. (A6.1), it is then also possible to explain the fact that its coefficients add up to one, as shown by Eq. (A6.3). The values of $<\theta_{opt}>$ and α can then be determined as detailed above. It turns out that $<\theta_{opt}>$=1.2 and α=0.30, in agreement with Eq. (A6.1). The procedure leading to Eq. (A6.1), anyway, shows that Eqs. (A6.3) and (A6.4) are exact solutions and not merely first order approximations.

One can also use Eq. (A6.3) without knowing α by assuming, as a first approximation, that α=½. By Taylor approximation, then, it easy to show that the arithmetic mean can be approximated with the geometric mean. For T<100 °C, at 5%:

$$T_{opt} \approx \sqrt{T_0 \cdot T_\infty} \quad \text{(A6.5)}$$

The temperature for which θ=1, T_c, is seen to be slightly different from T_{opt}:

$$T_c = T_{opt} + \partial_\theta T_{opt}(\theta_{opt}) \cdot (\theta_c - \theta_{opt}) = T_{opt} + (T_\infty - T_0) \cdot \alpha \cdot (1 + log(\alpha)) \quad \text{(A6.6)}$$

where Eqs. (A6.3)-(A6.4) were employed. By further applying Eq. (A6.3), one has:

$$T_c = (1-\tilde{\alpha}) \cdot T_\infty + \tilde{\alpha} \cdot T_0 \quad \text{(A6.7)}$$

where:

$$\tilde{\alpha} = -\alpha \cdot log(\alpha) \quad \text{(A6.8)}$$

Putting α=0.30 in Eqs. (A6.7) and (A6.8), one obtains:

$$T_c = 0.64 \cdot T_\infty + 0.36 \cdot T_0 \quad \text{(A6.9)}$$

Finally, let us notice that the assumption θ=1 simplifies calculations. Furthermore, it was verified that, at least in the 20-100 °C range, Eqs. (A6.1) and (A6.9) differ by 1.4%, at worst. Eq. (A6.9) is the result reported in the paper (where, with a slight notational abuse, Tc was renominated as T_{opt}).

ANNEX A7
PRESSURE DROP - MINIMUM FLUIDIZATION

Let us calculate the pressure drop experienced by the fluid and the fixed bed fluidization velocity. The concept

of minimal fluidization velocity originates from the fact that, beyond such a velocity, one has a fluidized bed, with an unstable behaviour (formation of channels where the fluid does not interact) for particle diameters ≥1 cm [Holdich, 2002]. Let us first consider a fixed bed. The pressure drop, for a laminar fixed bed with circular baffles, is indeed given by [Holdich, 2002]:

$$\Delta p_{fb} = 180 \cdot \frac{\epsilon_3^2}{(1-\epsilon_3)^3} \cdot \frac{\mu_f \cdot v_f \cdot h_c}{d_u^2} \quad \text{(A7.1)}$$

where ε_3 is the sphere packing density, μ_f the fluid velocity, v_f the average interstitial fluid velocity, h_c the bed height and d_u the unit diameter. The pressure drop is a monotonically increasing function of the sphere packing density and ε_3=0.74, the maximum possible value [Holdich, 2002], was assumed, so as to be on the safe side. By assuming d_u=1 cm, h_c≤20 cm, v_f≤2.3 m/s [MOXOFF, 2012b], a maximum pressure drop ~5 mbar (μ_f=1.8·10-5 kg/m·s [Biyikoglu, 2002]) is calculated. The pressure drop is then ~0.5% of the atmospheric pressure, at worst.

Let us come to the shell-and-tube exchanger. The expression for the pressure drop of the heat exchanger [Shah et al., 1998] is made up additive terms. It was verified that the terms describing baffle influence are dominating and:

$$\Delta p_{hh} = N_b \cdot (2 + 0.6 \cdot \widetilde{N_r}) \cdot \frac{\rho_f \cdot v_f^2}{2} + 4 \cdot f \cdot \widetilde{N_r} \cdot (N_b - 1) \cdot \frac{\rho_f \cdot v_f^2}{2} \quad \text{(A7.2)}$$

where N_b is the number of baffles $\widetilde{N_r}$ is an effective number of tube rows, Eq. (A7.3), ρ_f the fluid density, v_f the interstitial fluid velocity, f the friction factor (one has ≤0.3 for Re≥120 [Fernandez et al., 2010]). In Eq. (A7.2), $\widetilde{N_r}$ is given by [Shah et al., 1998]:

$$\widetilde{N_r} = \frac{0.05 \cdot d_c}{d_u} \quad \text{(A7.3)}$$

where d_c is the cylindrical module diameter and d_u is the unit diameter.

Eq. (A7.3) was derived from [Shah et al., 1998] under the hypothesis that the baffle cut (cylinder diameter minus baffle height) be 0.05 times the cylinder diameter and the tube pitch (the minimum distance between tubes) be 1.25 times the cylinder diameter [MOXOFF, 2012b]. Since one has d_c=50, d_u=5 mm [MOXOFF, 2012b], then $\widetilde{N_r}$=5. Assuming N_b=8 and v_f=2.3 m/s [MOXOFF, 2012b], Eq. (A7.3), with ρ_f =1.2 kg/m3 [Biyikoglu, 2002], gives a pressure drop of ~3 mbar or ~0.3% of the atmospheric pressure, at worst.

Let us finally come to the minimal fluidization velocity for a fixed or fluidized bed. This quantity is given by [Holdich, 2002]:

$$v_{mf} = \frac{1}{180} \cdot \frac{(1-\epsilon_3)^3}{\epsilon_3} \cdot \rho_m \cdot g \cdot \frac{d_u^2}{\mu_f} \quad \text{(A7.4)}$$

where ρ_m is the material density, g is the gravitational acceleration. Let us notice that the minimum fluidization velocity is a monotonically decreasing function of the sphere packing density, so that ε_3=0.74, the maximum possible value [Hales et al., 2006], was cautiously assumed. Since, for any material, ρ_m>765 kg/m^3 (see Tab.3) and g=9.8 m/s^2, one then has v_{mf}>5.5 m/s. Since from model simulations one gets v_f<2.3 m/s [MOXOFF, 2012b], the packed bed works out of the minimum fluidization regime and is therefore a fixed bed, as previously stated.